Rainfall Morphology in Florida Convergence Zones: A Numerical Study

J. MARSHALL SHEPHERD

Laboratory for Atmospheres, NASA Goddard Space Flight Center, Greenbelt, Maryland

BRAD S. FERRIER

National Center for Environmental Prediction/Environmental Modeling Center, Washington, D.C.

PETER S. RAY

Department of Meteorology, The Florida State University, Tallahassee, Florida

(Manuscript received 14 January 2000, in final form 6 June 2000)

ABSTRACT

Central Florida is the ideal test laboratory for studying convergence zone–induced convection. The region regularly experiences sea-breeze fronts and rainfall-induced outflow boundaries. The focus of this study is convection associated with the commonly occurring convergence zone established by the interaction of the sea-breeze front and an outflow boundary. Previous studies have investigated mechanisms primarily affecting storm initiation by such convergence zones. Few have focused on rainfall morphology, yet these storms contribute a significant amount of precipitation to the annual rainfall budget. Low-level convergence and midtropospheric moisture have been shown to be correlated with rainfall amounts in Florida. Using 2D and 3D numerical simulations, the roles of low-level convergence and midtropospheric moisture in rainfall evolution are examined.

The results indicate that area- and time-averaged, vertical moisture flux (VMF) at the sea-breeze front–outflow convergence zone is directly and linearly proportional to initial condensation rates. A similar relationship exists between VMF and initial rainfall. The VMF, which encompasses depth and magnitude of convergence, is better correlated to initial rainfall production than surface moisture convergence. This extends early observational studies that linked rainfall in Florida to *surface* moisture convergence. The amount and distribution of midtropospheric moisture affects how much rainfall associated with secondary cells develop. Rainfall amount and efficiency varied significantly over an observable range of relative humidities in the 850–500-mb layer even though rainfall evolution was similar during the initial or ''first cell'' period. Rainfall variability was attributed to drier midtropospheric environments inhibiting secondary cell development through entrainment effects. Observationally, a 850–500-mb moisture structure exhibits wider variability than lower-level moisture, which is virtually always present in Florida. A likely consequence of the variability in 850–500-mb moisture is a stronger statistical correlation to rainfall as noted in previous observational studies.

The VMF at convergence zones is critical in determining rainfall in the initial stage of development but plays a *decreasing* role in rainfall evolution as the system matures. The midtropospheric moisture (e.g., environment) plays an *increasing* role in rainfall evolution as the system matures. This suggests the need to improve measurements of depth and magnitude of convergence and midtropospheric moisture distribution. It also highlights that the influence of the environment needs to be better represented in convective parameterizations of larger-scale models to account for entrainment effects.

1. Introduction

Central Florida has the highest annual number of days with thunderstorms in the United States (Williams et al. 1992). Because of its unique geographical and meteorological conditions, Florida regularly experiences sea-breeze fronts (SBFs) and rainfall-induced, outflow boundaries (OBs). The convergence associated with these phenomena or interactions between them can provide lift to initiate convection. Lines of single-cell and multicell thunderstorms with heavy rainfall and frequent lightning that last 1–2 h are common. Numerous observational and modeling studies have addressed convection in Florida (Byers and Rodebush 1948; Day 1953; Gentry and Moore 1954; Frank et al. 1967; Pielke 1974; Ulanski and Garstang 1978; Burpee 1979; Simpson et al. 1980; Tripoli and Cotton 1980; Cooper et al. 1982; Holle and Watson 1983; Nicholls et al. 1991; Arrit 1993; Fankhauser et al. 1995; Kingsmill 1995; Halverson et al. 1996; Heymsfield et al. 1996; Wilson and Megenhardt 1997).

Corresponding author address: Dr. J. Marshall Shepherd, Laboratory for Atmospheres, NASA Goddard Space Flight Center, Greenbelt, MD 20771.
E-mail: shepherd@agnes.gsfc.nasa.gov

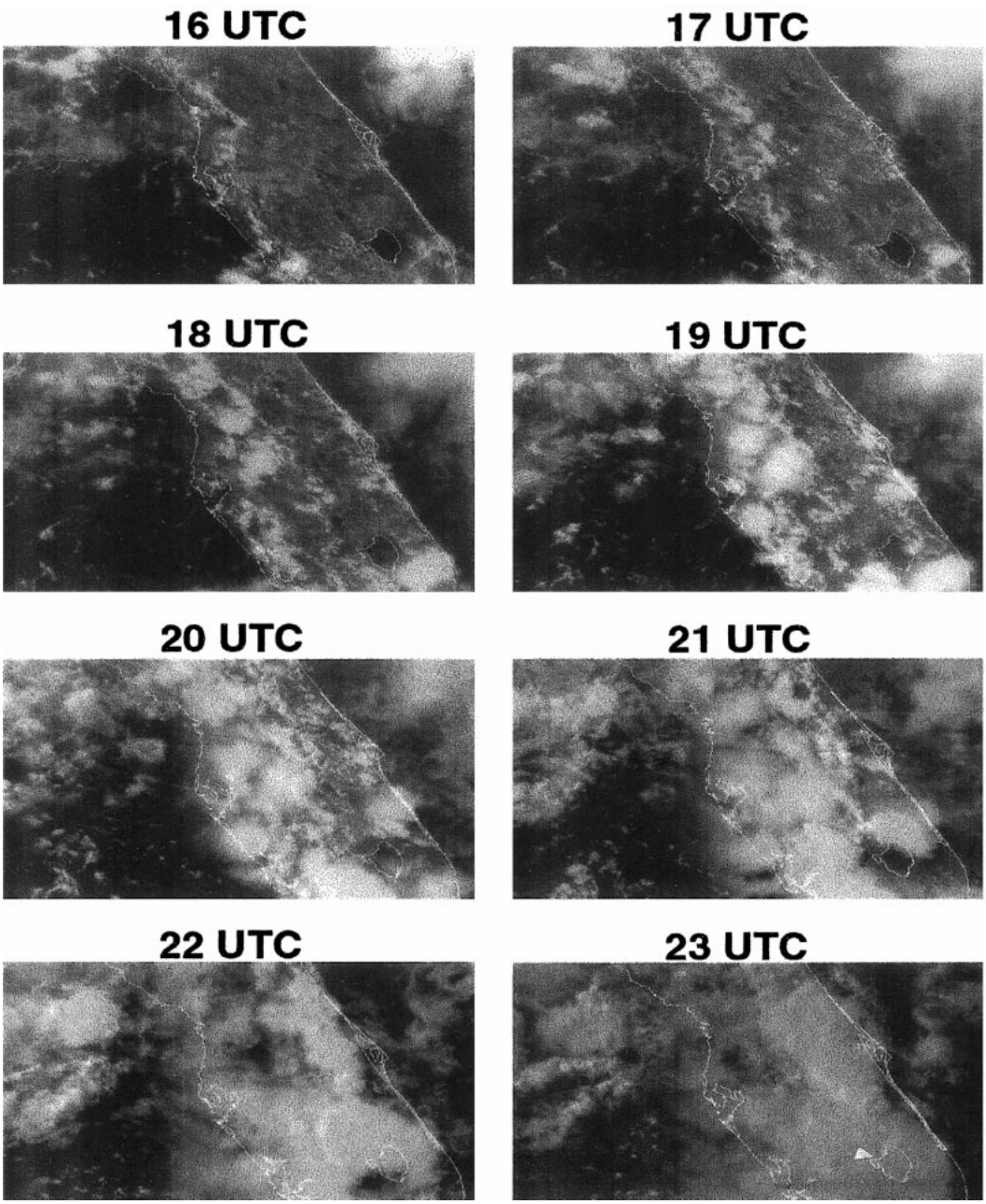

FIG. 1. Time history of visible GOES satellite imagery on 27 Jul 1991 in central Florida (22 UTC = 2200 UTC).

Blanchard and Lopez (1985) identified three primary types of wind flows in the Florida summertime regime. Type I days are characterized primarily by an easterly component that causes the east coast SBF to propagate inland while the west coast SBF remains stationary. Type II days are characterized by an even stronger easterly component. Type III days are characterized by a westerly component that results in the greatest amount of convective activity in eastern Florida. This is primarily due to the east coast SBF remaining essentially stationary, while the west coast front and outflow boundaries interact with it. Figure 1 is a time history of visible satellite imagery over central Florida on 27 July 1991 illustrating a typical type III day. Convergence zone–induced lines of convection are prevalent in summertime Florida regardless of the prevailing wind flow.

Prior studies have focused mainly on the synoptic- and mesobeta-scale (50–200 km) organization of convection forced by convergence zones and, to a lesser extent, the storm-/mesogamma-scale (1–50 km) organization. Although most of these studies have investi-

gated factors primarily affecting storm initiation, few have focused on rainfall evolution in Florida storms. Any broad understanding of rainfall in Florida should consider small convective systems since they can contribute up to 40% of Florida's total annual rainfall. The National Aeronautics and Space Administration's Tropical Rainfall Measuring Mission (TRMM) has established an extensive ground validation (GV) effort to understand tropical rainfall and its impact on global climate (Simpson et al. 1996). Central Florida is a primary GV site such that a study investigating rainfall morphology in Florida is relevant to TRMM science objectives.

Previous studies suggest that rainfall in Florida systems may be linked to surface convergence or midtropospheric moisture. Byers and Rodebush (1948), Ulanski and Garstang (1978), and Tripoli and Cotton (1980) suggested that the amount of rainfall in Florida storms is correlated with areal extent and magnitude of *surface* convergence. However, recent findings suggest that surface convergence is a necessary but not sufficient condition to accurately correlate with rainfall production. Kingsmill (1995) examined a case in which an outflow boundary collided with a sea-breeze front during the Convective and Precipitation Electrification Experiment (CaPE) (Williams et al. 1992). He found no significant convective initiation or enhancement although favorable conditions (i.e., sufficient moisture, surface convergence, and instability) were present. He theorized that there was sufficient convergence but the depth over which it was occurring was not sufficient to force parcels to their level of free convection. Wakimoto and Kingsmill (1995) found a similar occurrence. Such recent findings are consistent with earlier studies. Moore (1982) argued that an integrated moisture convergence parameter accounting for depth was more useful than a surface-based moisture convergence parameter for delineating severe storm and heavy rain events. Crook (1996) provided evidence in his model simulations of a convergence zone system that an integrated moisture convergence parameter may have been more effective at identifying rainfall evolution. Xin and Reuter (1996) found that the amount of rainfall in a convective system was sensitive to magnitude and depth of convergence.

Other investigators have correlated rainfall in Florida with midtropospheric moisture (i.e., 850–500 mb). Frank and Smith (1968) found that the strongest correlation between percentage of radar echo and meteorological parameters was midtropospheric moisture, specifically 700–500 mb. Burpee (1979) found that variations in surface convergence could not explain the large differences in daily averaged rainfall, but midtropospheric moisture could. Lopez et al. (1984) and Watson and Blanchard (1984) provided evidence that ''wet'' days were more correlated with midtropospheric moisture. Burpee (1989) illustrated that on a rare summer day in Florida, there was virtually no convective rainfall throughout the entire peninsula due to an unusually dry middle troposphere. Watson et al. (1991) correlated 700–500-mb moisture with increased occurrences of lightning-producing storms. Fuelberg and Biggar (1994) found the largest variability in relative humidity for convective–nonconvective days was in the 700–500-mb layer.

This study sought to provide a framework to couple low-level convergence and midtropospheric moisture to explain how they produce the most efficient rainfall system in the Florida convergence zone environment. A cloud–mesoscale model was employed to evaluate the sensitivity of rainfall morphology (i.e., life cycle, amount, and efficiency) to magnitude of convergence, depth of convergence, and 850–500-mb moisture structure. This research contributes to and extends the current base of understanding of Florida convection in the following ways.

- The individual and synergistic roles of convergence magnitude, convergence depth, and midtropospheric moisture distribution are quantified in relation to rainfall morphology not just convective initiation at a convergence zone.
- Numerical model simulations at storm (convective) scale provide new information on precipitation efficiency and rainfall production in Florida convection.
- The relative roles of vertical moisture flux and midtropospheric moisture environment (through entrainment effects) on rainfall development at a convergence zone are quantified.

This article discusses the study's hypotheses in section 2. Section 3 describes the numerical cloud model used in the experiments. Section 4 outlines the research methodology employed. Results of the sensitivity experiments, trajectory analysis, and conceptualizations are presented in section 5. Section 6 provides a summary and concluding remarks.

2. Hypothesized factors affecting rainfall production in Florida convection

Byers and Braham (1949), Browning et al. (1976), and Fovell and Tan (1998) have indicated that small convective thunderstorms (~1 h life cycle) consist of one or more individual convective cells. Browning et al. (1976) provided a classic illustration of the stages of development in a multicellular system. Weisman and Klemp (1982) found that the ratio of buoyant energy and vertical wind shear, bulk Richardson number, is a good indicator of storm type. In Florida, the bulk Richardson number often falls into the category favorable for multicellular development (Wilson and Megenhardt 1997).

It is hypothesized that rainfall produced by the initial convective cell is directly proportional to area- and time-averaged vertical moisture flux (VMF) at the convergence zone over a given time period prior to rainfall onset (McIlveen 1986; Xin and Reuter 1996). For the

purpose of this study, VMF (2D) at a convergence zone [i.e., over the depth below the lifted condensation level (LCL)] is derived from the anelastic continuity equation. The VMF (in units of kg m^{-2} s^{-1}) at the convergence zone can be represented as

$$VMF \cong \overline{\rho q M_{CZ}} Z_{CZ}, \quad (1)$$

where q is mixing ratio, ρ is a density term, M_{CZ} is convergence magnitude over the specified depth, and Z_{CZ} is convergence depth. Since density, mixing ratio, and convergence magnitude vary with height, the overbar represents the average of the product over the depth Z_{CZ} in the convergence zone region. Equation (1) essentially represents the integrated moisture convergence at the zone without advective effects due to horizontal moisture gradients.

The justification for neglecting the advective terms is based on two factors. First, only magnitude and depth of convergence were varied in the study while the low-level moisture gradient was constant in the experiments. Second, aircraft and surface observations from CaPE (see Fankhauser et al. 1995, Fig. 8) suggested that at the SBF–OB collision point the gradient in moisture may approach zero over a sufficient distance since mixing ratio is often similar behind the OB and SBF. Other assumptions were required in the derivation of VMF from the anelastic continuity equation. Meridional gradients were neglected since only two-dimensional experiments were considered for VMF calculations. Also, surface fluxes of moisture at the convergence zone were neglected. At the small timescales of this study (~1–90 min), VMF was much greater than surface fluxes of moisture. The mean VMF and surface moisture flux were computed over 10.0 km centered at the SBF–OB collision point at $t = 15$ min. The mean VMF and surface flux were approximately 42.4 kg m^{-2} s^{-1} and 0.1 kg m^{-2} s^{-1}, respectively.

The VMF was essentially altered by changes in the amount of moisture in the converging depth, the magnitude of convergence, and the depth of the convergence. The hypothesis is that early condensation rates should be directly proportional to the upward vertical moisture flux. This suggests a direct relationship between first-cell rainfall and VMF through the condensation rate–VMF proportionality.

It is further hypothesized that the amount and distribution of moisture in the middle troposphere (defined here as 850–500 mb) regulates the decay of the initial cell and the evolution of secondary cells. Based on the simulations described herein, rainfall produced by secondary cells is the primary contributor to total rainfall accumulation once the system transitions from the initial vertical moisture flux forcing in the first cell. The model runs indicated that a dry midtroposphere accelerates the decay of the initial cell and inhibits secondary cell development because of enhanced entrainment effects. The 850–500-mb layer is theorized to be an important source region for entraining air that affects secondary cell development. The effects of dry air entrainment on tropical convective clouds have been investigated for many years (e.g., Simpson 1983). The basic idea is that dry environmental air is entrained into the cloud and mixed with rising air parcels, leading to dilution of parcel buoyancy (Stommel 1947). Blyth (1993) presented a nice review of cloud entrainment processes and the difficulties quantifying them. To mitigate such difficulties, the *effects* of dry entrainment, (i.e., condensation and evaporation rates) were examined in this study. We suggest that growth of the first cell is linked to the vertical moisture flux forcing, while secondary cell growth and post–initial cell rainfall is primarily affected by environmental moisture in the midtroposphere.

TABLE 1. Key model parameters.

Model parameter	Description
dx, *dy*, horizontal resolution	500 m (2D), 1.0 km (3D)
dz, vertical resolution	500 m
dtsml, small time step	1 s
dtbig, big time step	10 s
Total model integration time (2D, 3D)	1.5 h
Lateral boundary conditions	Klemp–Wilhelmson-type radiation
Subgrid-scale mixing	1.5-order total kinetic energy (TKE) mixing closure
Computational mixing	Fourth-order mixing scheme
Rayleigh damping sponge	12–17 km
Microphysics	3-class ice with Kessler warm rain microphysics
Initialization	Cold pools (following Mueller et al. 1993)

3. Model

The numerical model employed in this study is the Center for Analysis and Prediction of Storms (CAPS) Advanced Regional Prediction System (ARPS) version 4.0. The ARPS model (Xue et al. 1995) is a modular system that contains many physical and numerical options and is capable of 1D, 2D, or 3D simulations. ARPS can resolve atmospheric systems on scales ranging from a few meters to hundreds of kilometers. Such flexibility makes simulations of smaller-scale phenomena like thunderstorms, outflow boundaries, and sea-breeze fronts possible. These phenomena are often parameterized or omitted in larger-scale models.

The model is a nonhydrostatic atmospheric prediction model based on the compressible Navier–Stokes equations describing atmospheric flow. The system of equations to be integrated contains nine prognostic equations, which include three momentum equations, the pressure and thermodynamic equations, moisture equations for various types of condensate, and a subgrid kinetic energy equation. Table 1 describes key model parameters used in the model.

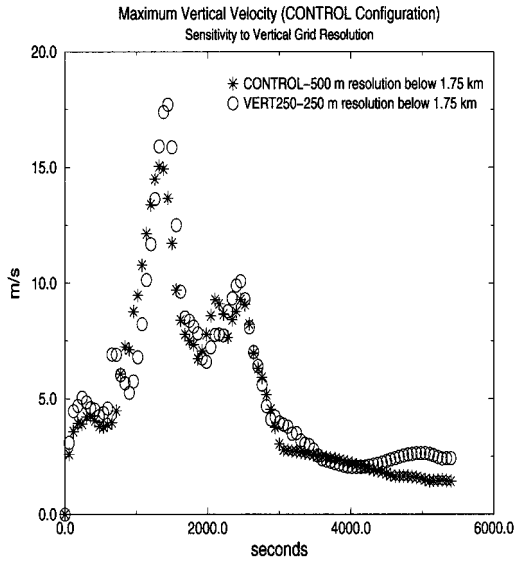

FIG. 2. Time series of maximum vertical velocity (m s^{-1}) in the domain for experiments CONTROL and VERT250.

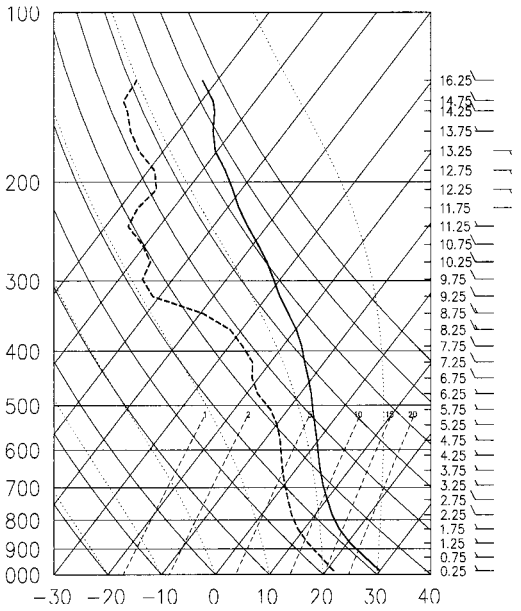

FIG. 3. Modified 1956 UTC 15 Aug 1991 Deerpark sounding (2D experiments): half barb = 2.5 m s^{-1}; full barb = 5.0 m s^{-1}.

Two-dimensional model configuration

Recently, Kingsmill (1995) and Fankhauser et al. (1995) documented the three-dimensional structure of the SBF–OB convergence zone environment. They found very sharp gradients in temperature, moisture, and wind. These gradients existed on scales ranging from a few hundred meters to 1.0 km. These observational studies provide the basis for the experiment configurations.

The model grid size was 80 km × 17 km in the 2D experiments. The grid interval was 500 m in the horizontal and vertical direction. Sensitivity tests executed with vertical resolutions of 250 and 500 m below 1.75 km were run to evaluate performance. Figure 2 illustrates slight differences in the evolution of maximum vertical velocity, but generally, the system evolution in both sensitivity experiments was quite similar. It is equally encouraging that the magnitude of the velocities was consistent with vertical velocities observed in recent studies of Florida convection (e.g., Yuter and Houze 1995; Sun and Crook 1998). Results provide confidence in our decision to use 500-m vertical resolution in the sensitivity experiments although future studies will employ finer resolution in the boundary layer to more thoroughly resolve shallow convergence zones.

The model was integrated for 1.5 h in time to capture the collision of the SBF and OB, initial formation of rainfall, maturation of the system, and decay of the system. The thermodynamic profile used for initialization is *based* on the 1956 UTC 15 August 1991 Deerpark CaPE sounding (Fig. 3). On this day, active convection associated with an SBF–OB interaction occurred (Yuter and Houze 1995). However, the moisture profile was altered such that relative humidity at each grid level between 850 and 500 mb was 60%. A mean of 60% was chosen based on Fuelberg and Biggar's (1994) study, which found that midtropospheric moisture in Florida was generally near 60% but could vary by as much as 40%. Adjusting the 850–500-mb moisture to 60% facilitated easier comparisons with experiments in which moisture was altered in the layer.

The initial SBF (Simpson 1987) and OB (Charba 1974) were modeled as density currents approaching from the eastern and western portions of the domain, respectively. The density currents were inserted as linear profiles of potential temperature perturbation and wind speed, decreasing with height as in Mueller et al. (1993). They were inserted at opposite ends of the domain. Figure 4 provides an indication of how the u component of the wind in the density currents varied for selected experiments. It is these variations that establish the variations in VMF. The depth, kinematic conditions, and thermodynamic compositions were based on Kingsmill (1995) and Fankauser et al. (1995). Kingsmill (1995) used Cross-chain Linked Atmospheric Sounding System soundings placed within an SBF and an OB. He found that the OB reached depths of 1.7 km. The SBF was ~0.7 km. Kingsmill (1995) and Fankhauser et al. (1995) found using detailed Portable Automated Mesonet data and low-flying aircraft data that the ambient temperature deficit behind the SBF ranged from 1° to 3°C, while the ambient temperature deficit behind the OB ranged from 2° to 10°C. In general, the sea-breeze front air was roughly 1.0–2.0 g kg^{-1} moister than the intermediate or OB air.

For the outflow boundary, the leading edge of the density current was prescribed roughly 20 km from the

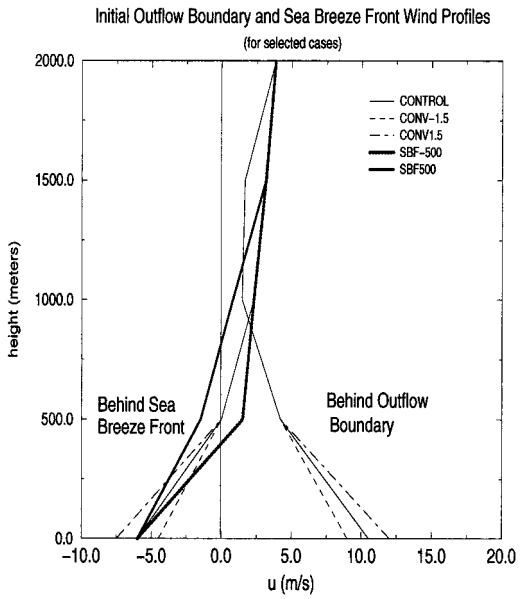

FIG. 4. Examples of initial, model wind profiles (m s^{-1}) behind the sea-breeze front and outflow boundary for selected experiments. Profiles that are less (greater) than 0.0 at the surface represent sea-breeze fronts (outflow boundaries).

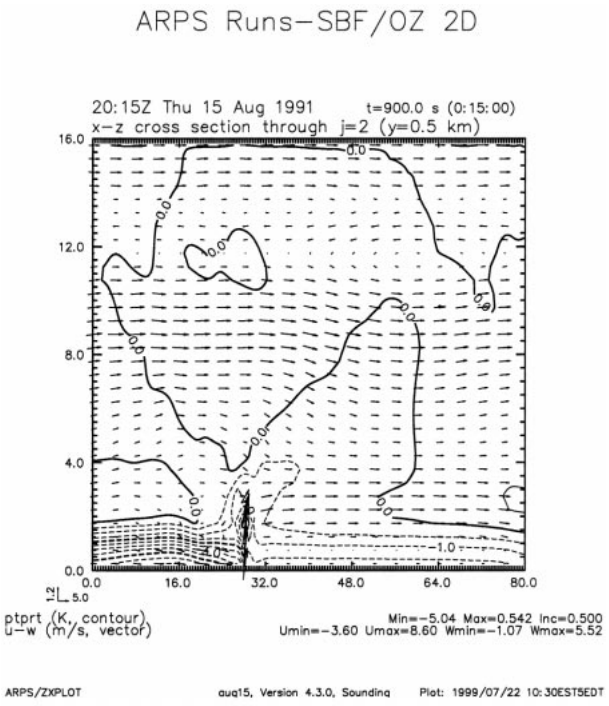

FIG. 5. Configuration of sea-breeze front and outflow boundary at $t = 15$ min in 2D control run. The plot is an overlay of perturbation potential temperature (K) and wind vectors (m s^{-1}). The collision point of the two density currents is near $x = 30.0$ km.

western lateral boundary. It had a mean perturbation potential profile that decreased from ~ -8.0 K to 0.0 at 1.7 km. Mueller et al. (1993) noted that this type of profile was closer to the real vertical structure of outflow boundaries. Additionally, Chen (1995) found that the model performed better with linear profiles, especially near the top of the cold pool. He found that specifying a uniform temperature perturbation created spurious circulations near the top of the cold pool. The resulting outflow boundary (density current) propagated eastward with a mean potential temperature deficit of -4.0 K.

A similar configuration was used to model the sea-breeze front except the leading edge of the density current was placed 40 km from the eastern boundary. In addition, the mean potential temperature deficit was only -1.5 K (e.g., decreasing from -3.0 K at the surface to 0.0 K near 0.7 km). Figure 5 is the 2D configuration of the perturbation potential temperature associated with the theoretical OB and SBF at $t = 15$ min of simulation time in the CONTROL run. The SBF is the more shallow density current with surface easterly flow on the right side of the domain. The outflow boundary is the deeper density current with westerly flow on the left side of the domain. The SBF and OB collide at $t \cong 15$ min at grid point $x \cong 28$ km for the CONTROL run.

4. Research methodology

The research was set within the framework of the Florida CaPE environment *though the study investigates theoretical system development as opposed to specific case study days.* The two-dimensional experiments were designed so that the variability of the parameter in question was within the dynamic range of variability observed near typical sea-breeze front–outflow boundary convergence zones in central Florida (Kingsmill 1995). Two sets of 2D experiments were conducted to determine the sensitivity of the rainfall evolution to 1) convergence magnitude and depth and 2) midtropospheric moisture distribution. Each of the sensitivity experiments was compared to a control experiment based on the sounding in Fig. 3. Three-dimensional experiments were investigated as a sanity check on the two-dimensional work and were not meant to be exhaustive. The discussion will focus primarily on the two-dimensional results. Three dimensional results will be discussed in future work.

a. Integrated convergence experiments (2D)

The integrated convergence experiments were designed to ascertain whether initial rainfall is directly related to a parameter defined as the area- and time-averaged VMF below the (LCL). Keeping the initial moisture profile constant, the VMF was altered by changing the depth or magnitude of convergence. Two experiments were included to elucidate the relative significance of convergence depth versus surface convergence magnitude. Table 2 describes the integrated convergence experiments.

TABLE 2. Description of the 2D integrated convergence experiments: SBF = sea-breeze front; OB = outflow boundary.

Experiment	Description
CONTROL	CONTROL
Magnitude	
CONV1.5	Increase surface layer winds behind SBF and OB by 1.5 m s^{-1} (similar to Lee et al. 1991)
CONV-1.5	Decrease surface layer winds behind SBF and OB by 1.5 m s^{-1} (similar to Lee et al. 1991)
Depth	
SBF-500	Decrease SBF depth by 500 m
SBF500	Increase SBF depth by 500 m
OB-500	Decrease OB depth by 500 m
OB-500SBF500	Decrease OB depth by 500 m, increase SBF by 500 m
Magnitude and depth	
CONV-1.5SBF500	Decrease surface layer winds by 1.5 m s^{-1}, increase SBF depth by 500 m
CONV1.5SBF-500	Increase surface layer winds by 1.5 m s^{-1}, decrease SBF depth by 500 m

The integrated convergence experiments were designed such that the changes in surface layer wind were within typical variability at an SBF or OB (Lee et al. 1991; Fankhauser et al. 1995). The depth experiments were also designed based on previous studies. The variability of the SBF depth ($\pm$500 m) was based on reports of the sea-breeze front being relatively shallow ($\sim$200 m) as in Rao et al. (1999) to being relatively deep ($\sim$700–1000 m) as in Kingsmill (1995). The variability of the OB depth ($-$500 m) was based on studies such as Droegemeier and Wilhelmson (1985), Lee et al. (1991), and Kingsmill (1995), in which OB depth varied from a few hundred meters to 1700 m. Since few investigators have reported OB depths on the order of 2200 m in Florida, a case in which the OB depth was increased by 500 m was not conducted. The main goal was to create variability in convergence depth and magnitude that is within reasonable dynamic range of observations.

b. Midtropospheric moisture experiments (2D)

The midtropospheric (850–500 mb) moisture experiments were designed to investigate how amount and distribution of midlevel moisture affect precipitation efficiency and rainfall production. These experiments tested observational findings that midtropospheric moisture exhibits the strongest correlation to rainfall in Florida. Figure 6 illustrates the soundings as modified for each sensitivity experiment. Table 3 describes the midtropospheric moisture experiments. Air parcel trajectories were computed, using the technique of Tao et al. (1995). The trajectory analyses were used to supplement findings in the midtropospheric moisture experiments in terms of entrainment effects.

c. Analysis parameters

1) STRUCTURE AND EVOLUTION

The evolution and morphology of the convective rainfall systems were investigated qualitatively using model calculated vertical velocity, mixing ratio perturbations, convective available potential energy (CAPE), and equivalent potential temperature. The primary low-level convergence parameters investigated were area- and time-averaged vertical moisture flux ($\langle$VMF$\rangle$) at 1.5 km and area- and time-averaged surface moisture convergence ($\langle$SMC$\rangle$) at the SBF–OB convergence zone. Both $\langle$VMF$\rangle$ and $\langle$SMC$\rangle$ were calculated from $t = 15$ to $t = 25$ min of model run time as mean values over a 10-km area centered on the approximate collision point of the SBF and OB. The brackets ($\langle \cdot \rangle$) represent area- and time-average. Experience from test runs suggested that a 10.0-km region was sufficient to resolve the low-level convergence at the SBF–OB collision point and its minimal movement during the initial 30 min after collision.

2) QUANTITATIVE PRECIPITATION AMOUNTS

The *total accumulated rainfall* (expressed in kg km^{-1}) was defined as the total amount of rainfall in the model domain over the time integration of the model. The *first-cell accumulated rainfall* (expressed in kg km^{-1}) was defined as the amount of rainfall that accumulated from the beginning of the run to a specific time after the relative minimum (i.e., roughly 40 min in this study) in condensation rate following the initial peak in that rate, as shown in Fig. 7. This parameter was arbitrarily defined to give some measure of first cell rainfall although some first cell contributions are likely to occur after 40 min.

3) WATER BUDGETS

The budget of condensed water integrated over space and time in the full model domain is

$$C = E + R + S, \tag{2}$$

where C is total condensation plus deposition of all ice species, E is total evaporation plus sublimation of ice, R is the total rainfall at the surface, and S is the mass of suspended condensate. Equation (2) followed Ferrier et al. (1996) and assumed no flux through the volume boundaries. *Precipitation efficiency* (PE) was calculated similarly to Ferrier et al. (1996):

$$\mathrm{PE} = R/C. \tag{3}$$

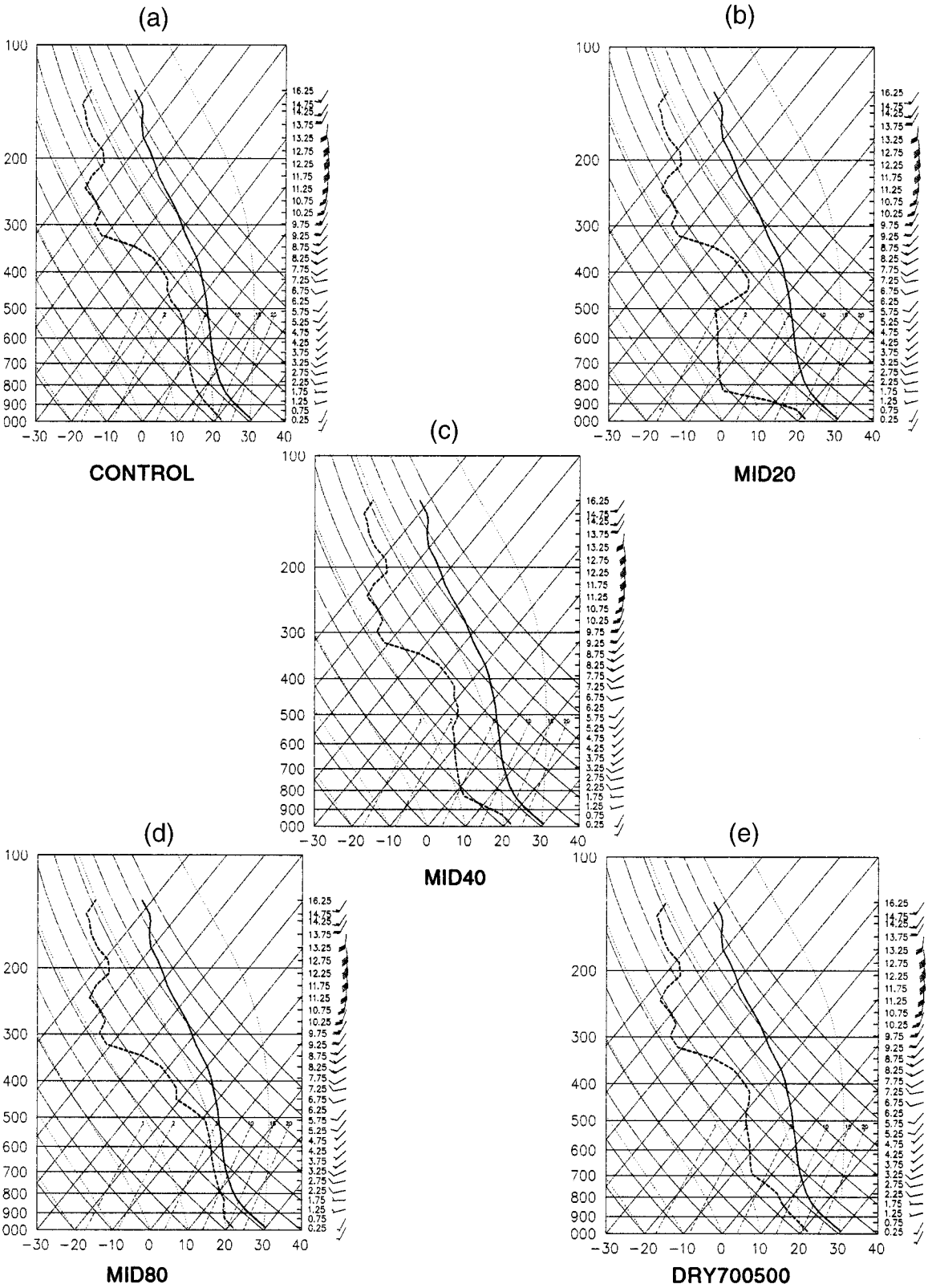

FIG. 6. Soundings used in the midtropospheric sensitivity experiments: half barb = 2.5 m s^{-1}; full barb = 5.0 m s^{-1}.

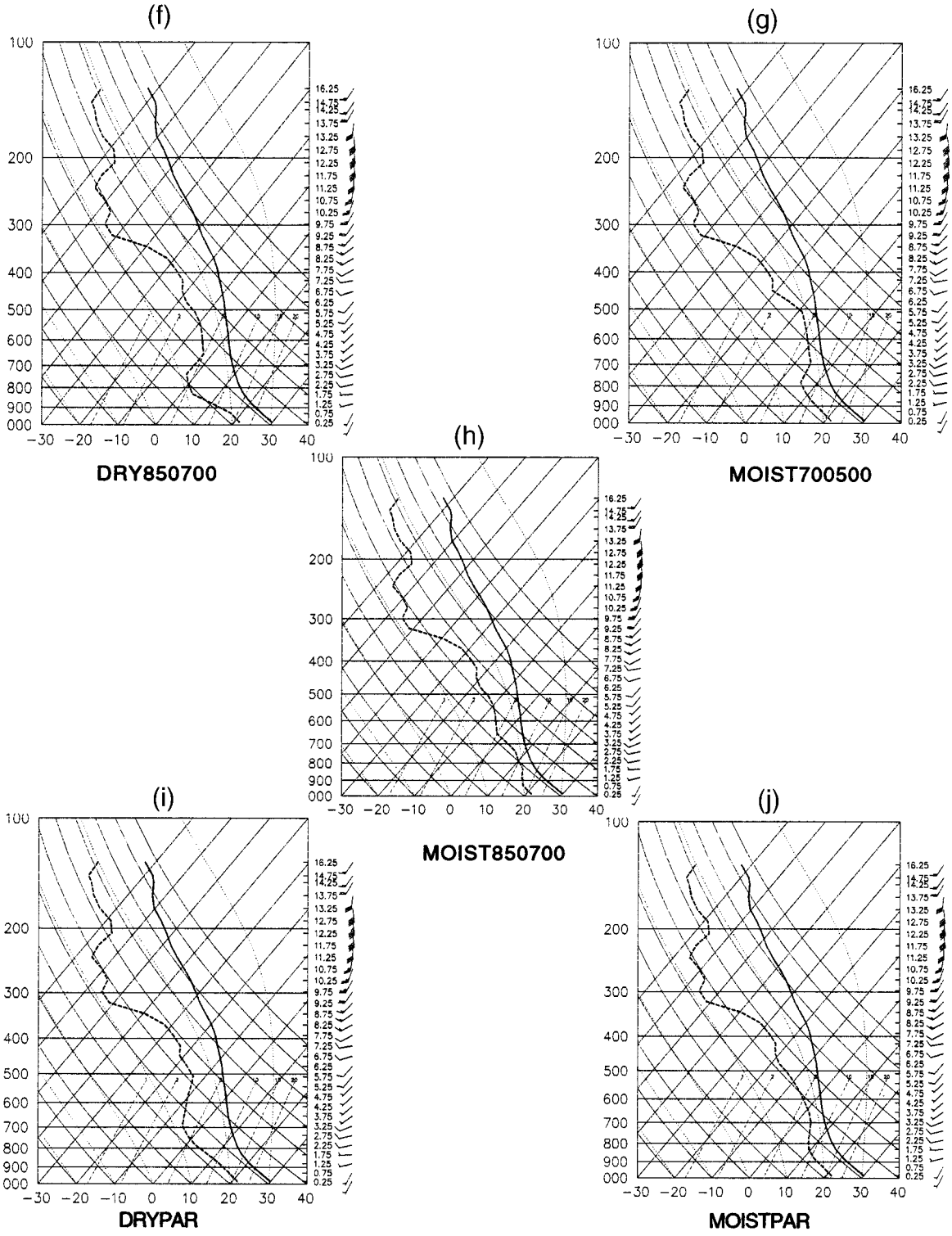

FIG. 6. (*Continued*)

TABLE 3. Description of the 2D midtropospheric moisture experiments.

Experiment	Description
CONTROL	CONTROL
Bulk	
MID20	Decrease 850–500-mb relative humidity to 20%
MID40	Decrease 850–500-mb relative humidity to 40%
MID80	Increase 850–500-mb relative humidity to 80%
Distribution	
MOIST700500	Increase 700–500-mb relative humidity to 80%
MOIST850700	Increase 850–700-mb relative humidity to 80%
MOISTPAR	Increase 850–500-mb relative humidity as a parabolic function peaking at 700 mb
DRY700500	Decrease 700–500-mb relative humidity to 40%
DRY850700	Decrease 850–700-mb relative humidity to 40%
DRYPAR	Decrease 850–500-mb relative humidity as a parabolic function peaking at 700 mb

The microphysics package was structured such that time series and vertical profiles of *condensation, evaporation,* and *net condensation* could be analyzed. *Net condensation* (NC) is

$$\mathrm{NC} = C - E. \tag{4}$$

Water budget constituents and rainfall amounts were only considered for a portion of the domain that encompassed the parent convective storm. This subdomain resolved initial and secondary cell development but excluded spurious growth of cumulus clouds significantly distant from the parent storm. These small cumulus clouds were related to outflow features downstream and near the lateral boundaries and did not produce rainfall.

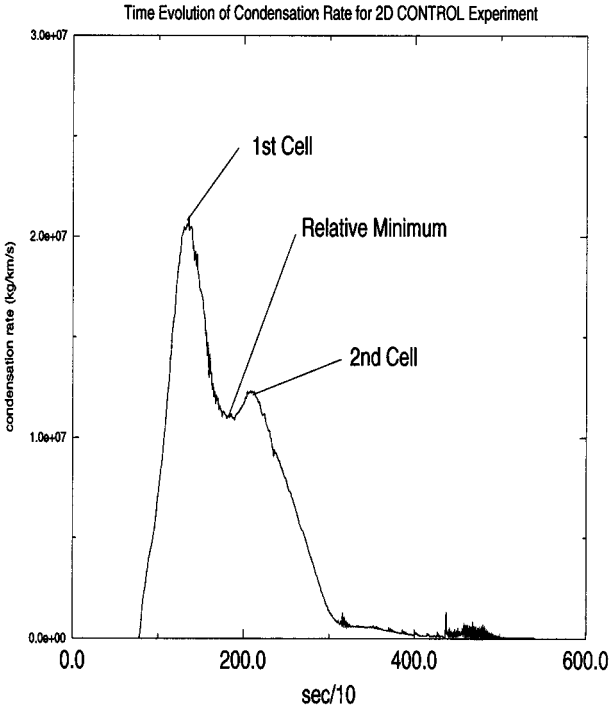

FIG. 7. Time series of condensation rate (kg km^{-1} s^{-1}) for 2D CONTROL experiment. The transition period from exclusively first cell rainfall to secondary cell rainfall is located in the relative minimum.

The parent storm was relatively stationary in relation to the initial sea-breeze front–outflow boundary convergence zone. The subdomain was centered at the collision point and was 20 km wide in order to resolve downstream secondary cells of the parent system. Figure 8 diagrams the subdomain used in the study and illustrates typical cells within the domain and spurious convection outside of the analysis domain. Lessons from several experimental runs provided assurance that the multicellular activity of the parent storm was captured within the subdomain.

5. Results

a. Two-dimensional integrated convergence experiments

Table 4 summarizes characteristics of the initial convection associated with the nine integrated convergence experiments. The table lists ⟨SMC⟩, ⟨VMF⟩, and CAPE at the initialization time. Table 4 also includes total surface rainfall and condensation from the first convective

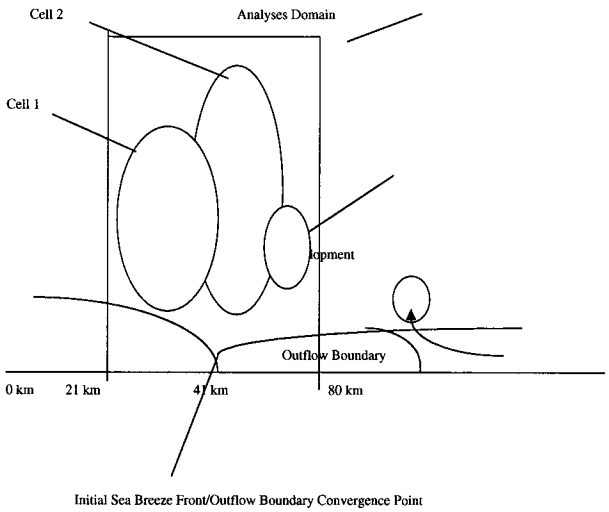

FIG. 8. Conceptualization of the subdomain (e.g., the enclosed box) used for water budget calculations and rainfall analyses. Cell 1 is the oldest cell. Cell 3 is the youngest cell.

TABLE 4. The name of the experiment; the time-averaged, mean surface moisture convergence (⟨SMC⟩) at the collision point; the time-averaged, mean vertical moisture flux (VMF) at the collision point; CAPE; total domain accumulated surface rainfall from the first convective cell (kg km^{-1}); and total domain condensation (kg km^{-1}) from the first convective cell. Duration of the initial cell is defined in section 4.

Expt	⟨SMC⟩ (g kg^{-1} s^{-1}) × 10^3	⟨VMF⟩ (kg m^{-2} s^{-1}) × 10^3	CAPE (J kg^{-1})	Initial rainfall (kg km^{-1}) × 10^8	Initial condensation (kg km^{-1}) × 10^8
CONTROL	44.4	290.5	1843	2.6	16.3
Magnitude					
CONV1.5	46.5	333.3	1843	3.4	19.1
CONV-1.5	41.0	235.5	1843	1.9	13.7
Depth					
SBF500	44.6	332.0	1843	3.4	17.7
SBF-500	42.6	268.0	1843	2.2	15.0
OB-500	41.6	284.6	1843	2.3	14.8
OB-500SBF500	42.5	329.3	1843	3.0	16.1
Magnitude and depth					
CONV-1.5SBF500	42.0	284.6	1843	2.6	15.5
CONV1.5SBF-500	45.6	313.0	1843	3.0	17.7

cell (see section 4). Generally, the experiments with larger ⟨VMF⟩ relative to CONTROL were associated with increased convergence magnitude at the surface (e.g., CONV1.5, CONV1.5SBF-500) or increased depth of convergence (e.g., SBF500, OB-500, OB-500SBF500). Likewise, experiments with smaller ⟨VMF⟩ were associated with reduced convergence magnitude at the surface (e.g., CONV-1.5, CONV-1.5SBF500) or reduced convergence depth (e.g., SBF-500).

In terms of initial rainfall produced by the first cell, total rainfall accumulations ranged from 1.9×10^8 to 3.4×10^8 kg km^{-1}. This result indicates that sensitivity experiments produced increases in initial rainfall as large as 30% and decreases as small as 27% compared to CONTROL. Table 4 indicates that experiments with large values of ⟨VMF⟩ generally produced more rainfall in the first cell relative to CONTROL. Similarly, experiments with small values of ⟨VMF⟩ produced less rainfall than CONTROL.

A linear regression analysis was conducted to investigate the correlations between ⟨VMF⟩, ⟨SMC⟩, and total condensation and accumulated rainfall associated with the first convective cell. In the top panel of Fig. 9, ⟨VMF⟩ is shown to be correlated ($r = 0.88$) to the total condensation of the first cell. The middle panel of Fig. 9 illustrates a strong correlation ($r = 0.96$) between ⟨VMF⟩ and the initial rainfall accumulation. The bottom panel of Fig. 9 indicates that ⟨SMC⟩ exhibits a weaker correlation ($r = 0.80$) to initial rainfall accumulation. The weaker correlation between ⟨SMC⟩ and initial rainfall is primarily due to experiments CONV-1.5SBF500 and CONV1.5SBF-500. These experiments are examples of how inverse changes in depth and magnitude can offset each other. An increase (decrease) in surface magnitude may be offset by a decrease (an increase) in convergence depth such that ⟨VMF⟩ might remain essentially constant. A good example of depth–magnitude offset can be observed with CONV-1.5 and CONV-1.5SBF500. Both experiments possessed the same alteration of initial surface winds yet the ⟨VMF⟩ for CONV-1.5 is 16% less than CONV-1.5SBF500, which is compensated by deeper sea-breeze convergence.

The stronger correlations for ⟨VMF⟩ are a direct result of the parameter encompassing convergence magnitude and depth. This extends early studies like Ulanski and Garstang (1978) *and* Tripoli and Cotton (1980) *that linked Florida rainfall to surface convergence features.* This also explains why surface convergence may not be sufficient to explain forcing in the initial convective cell as Kingsmill (1995) found. Figure 9 indicates a direct, linear relationship between ⟨VMF⟩ and initial rainfall.

Figure 9 illustrates that vertical moisture flux is strongly linked to the initial rainfall through the condensation rate. Stronger ⟨VMF⟩ increases the condensation rate of the first convective cell, which leads to enhanced rainfall rates and larger accumulations. These relationships can be summarized as

$$\text{VMF} \propto \text{condensation rate}, C \propto \text{initial rainfall rates}.$$

Figure 10 is the time series of subdomain-averaged condensation rates during the first 30 min of model run time for each 2D integrated convergence experiment. The condensation rate in the upper panel of Fig. 10 illustrates that experiments with larger ⟨VMF⟩ (e.g., CONV1.5, SBF500, CONV1.5SBF-500) produced instantaneous condensation rates that were 10%–30% larger than CONTROL. Experiments with smaller ⟨VMF⟩ (e.g., CONV-1.5, SBF-500, OB-500) produced 10%–30% smaller instantaneous condensation rates. The experiments with larger ⟨VMF⟩ also peaked in condensation rate sooner than smaller ⟨VMF⟩ experiments, in some cases by as much as 3–5 min. The combined effect of more rapidly developing and larger condensation rates explains why the rain rates at $t = 30$ min were larger for experiments with larger ⟨VMF⟩. As raindrops grow at the expense of the excess cloud water, rain rates increase in proportion to the increased ⟨VMF⟩ forcing and condensation rates. This explains why mean domain rain rate in CONV-1.5 was roughly 23% less than CONTROL, while the rate for SBF500 was roughly 24% greater at $t = 1800$ s.

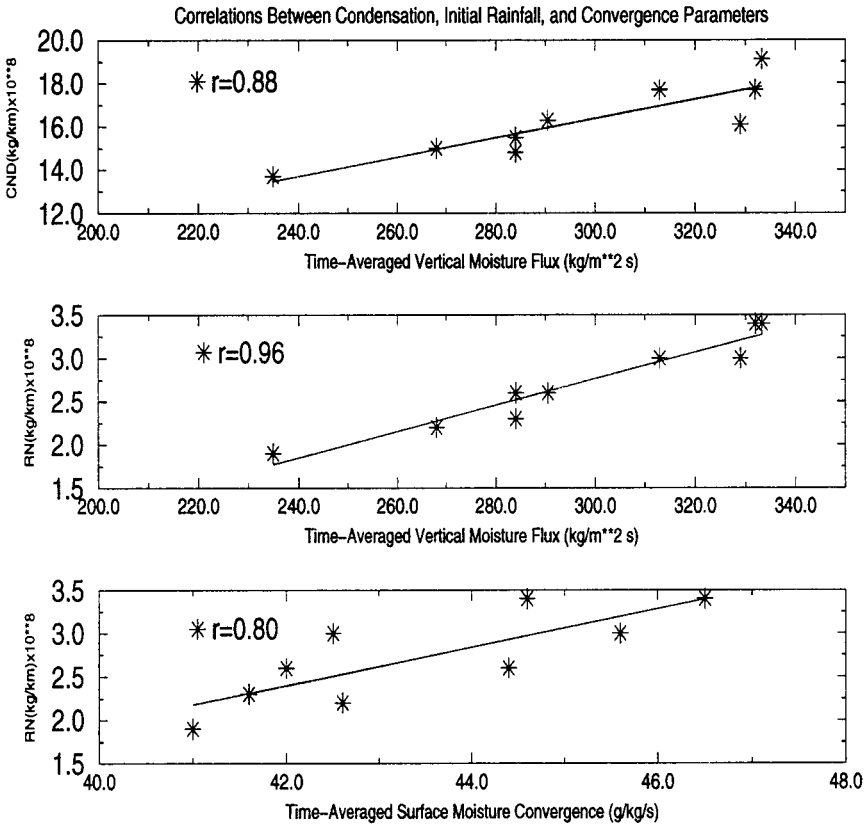

FIG. 9. Linear regression analysis of correlations between ⟨VMF⟩, ⟨SMC⟩, and total condensation and accumulated rainfall associated with the first convective cell: (top) ⟨VMF⟩ condensation, (middle) ⟨VMF⟩ rainfall, (bottom) ⟨SMC⟩ rainfall.

Figure 10 also illustrates an apparent lag of roughly 8–10 min between peak condensation rates (near 1300 s) and the peak rain rates (near 1800 s). It was observed that the relative minimum in condensation rate following the peak condensation rate coincided with the period of maximum rainfall intensity. This finding indicates that condensation processes in the first convective cell peaked on the order of 10 min prior to the most intense surface rain rates. Hondl and Eilts (1994) found that the time between first cell development (dB$Z > 10$) and dBZ values greater than 40 ranged from 5 to 45 min with the median time being 14 min.

b. Two-dimensional midtropospheric moisture experiments

The second component of our hypothesis argues that secondary cells, which develop in response to downdraft forcing from the initial cell, are regulated by the 850–500-mb moisture content. *The results suggest that the forcing–regulation relationship between vertical moisture flux and midtropospheric moisture may explain why a storm with similar convergent forcing may produce different rainfall totals on a given day.* To test the second component of our hypothesis, two sets of midtropospheric moisture experiments were conducted. One set of experiments investigated the sensitivity of rainfall evolution to bulk moisture changes in the 850–500-mb layer. Another set of experiments investigated the sensitivity of rainfall evolution to the distribution of moisture in the 850–500-mb layer.

1) BULK MOISTURE EXPERIMENTS

Table 5 describes some of the initial characteristics of the bulk moisture experiments. Table 6 lists various water budget terms and precipitation efficiency. In Table 6, results indicate that a dry (moist) 850–500-mb layer produced a convective system that precipitated less (more) total rainfall and was less (more) efficient. Experiment MID20 accumulated 42% less rainfall than CONTROL, while MID80 produced almost twice as much surface rainfall as CONTROL. In terms of PE, MID80 was 10% more efficient than CONTROL, while MID20 was 14% less efficient. This result is consistent with Burpee's (1989) deduction that a rare, ''no rain'' day in Florida was the result of a dry (~25% RH) midtroposphere. It is useful to recall that CONTROL had a mean relative humidity of 60%.

In general, the variability of PE ranged from 23% to

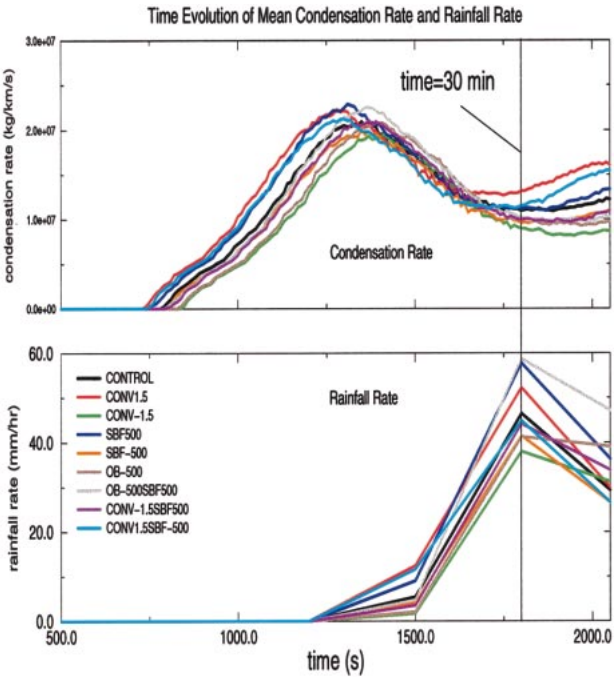

FIG. 10. Time series of mean condensation rate (kg km^{-1} s^{-1}) and mean rainfall rate (mm h^{-1}) during the first 35 min of model run time for each 2D integrated convergence experiment.

47% over the bulk moisture experiment parameter space. Braham (1952), using cloud data, found precipitation efficiencies in Florida storms to be near 19%. Ulanski and Garstang (1978) found precipitation efficiencies in small storms to range from 37% to 54%. *Neither investigator calculated PE values using total condensation and total surface rainfall as this study did.* They calculated PE using estimates of moisture inflow at cloud base or the surface.

Our hypothesis links variability in rainfall production to rainfall that is produced (or not produced) by secondary cellular development. If this is true, rainfall evolution in the initial cell period should be similar for each experiment. Figure 11 is the time evolution of PE in the bulk moisture experiments. In each experiment, the initial rainfall, inferred from PE evolution, evolved in roughly the same manner. This was concluded by noting that the time series coincided until roughly $t = 2000$ s. After this time, PE deviated as a function of the 850–500-mb moisture profile in the experiments. *This deviation suggests that rainfall production after initial VMF forcing of the first cell is a function of midtropospheric moisture.*

TABLE 5. A description of the experiment, the mean precipitable water (mm) of the 850–500-mb layer (initial), and the CAPE (J kg^{-1}) of the prestorm environment for the bulk moisture experiments.

Expt	Mean 850–500-mb precipitable water (mm)	CAPE (J kg^{-1})
CONTROL	18.7	1843
MID20	6.3	1816
MID40	12.5	1830
MID80	25.0	1857

TABLE 6. A description of the model results from the bulk moisture experiments in terms of total condensation/deposition (C), total evaporation/sublimation (E), total surface rainfall (R), total suspended condensate (S), and precipitation efficiency (PE).

Expt	C (kg km^{-1}) $\times 10^8$	E (kg km^{-1}) $\times 10^8$	R (kg km^{-1}) $\times 10^8$	S (kg km^{-1}) $\times 10^8$	PE (%)
CONTROL	23.4	14.5	8.8	0.02	37
MID20	21.6	16.4	5.1	0.01	23
MID40	23.8	16.3	7.4	0.08	31
MID80	31.3	16.2	14.8	0.16	47

Figure 12 plots vertical velocity and wind vectors at $t = 2100$ s for CONTROL, MID20, and MID80. This time was representative of the period that secondary cell evolution began. In MID20, a weaker cell (local centroid of vertical velocity) centered near $x = 32.0$ km and $z = 3.0$ km has developed. A more vigorous cell developed in MID80. The cell in MID20 was likely surpressed by increased entrainment effects due to the dry midtropospheric environment. We now investigate so-called entrainment effects to determine how they affect secondary cell development in the experiments.

The net condensation essentially provides a mechanism to see whether condensation or evaporative processes are dominant at a given time in the subdomain. A negative value indicates that evaporative processes are larger. Total suspended condensate is the sum of all

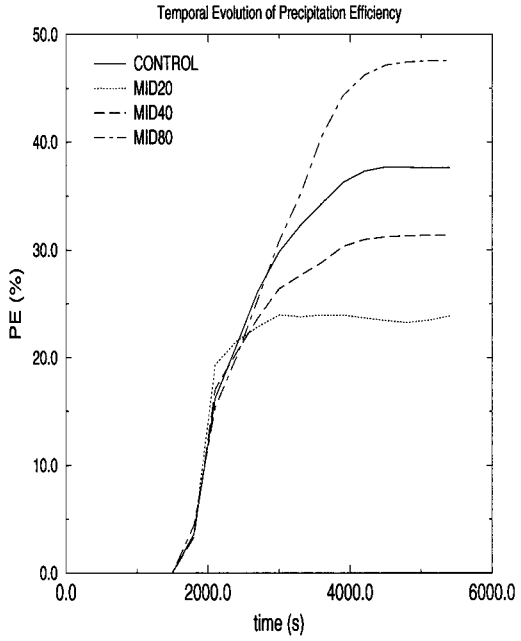

FIG. 11. Time evolution of precipitation efficiency (%) in the 2D bulk moisture experiments.

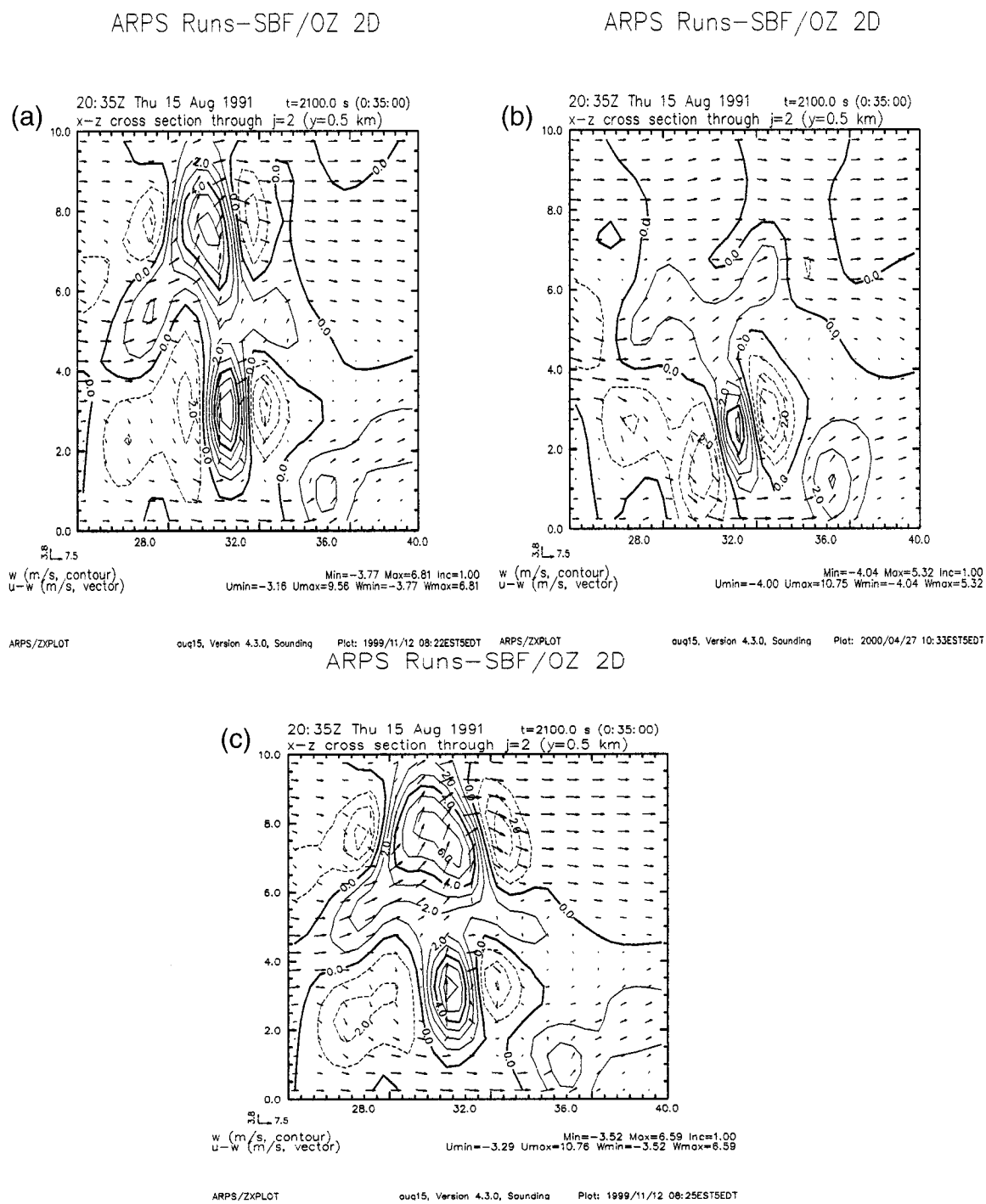

FIG. 12. Vertical velocity (m s^{-1}) and wind vectors at $t = 2100$ s for (a) CONTROL, (b) MID20, and (c) MID80. Updrafts associated with cells are identified as centroids of positive vertical velocity (solid lines). Dotted lines denote regions of negative vertical velocity (i.e., downdrafts).

hydrometeors (i.e., cloud water, rainwater, ice species) above ground level. Figure 13 illustrates that during the earliest stages of development the net condensation rate exhibited an inverse relationship to the amount of mid-level moisture. In other words, the drier experiments exhibited enhanced net condensation in the first 5–15 min after the SBF–OB collision. We hypothesize that this was related to enhanced downdrafts in the drier runs. The enhanced downdrafts temporarily fed the initial outflow boundary with cooler air that increased the

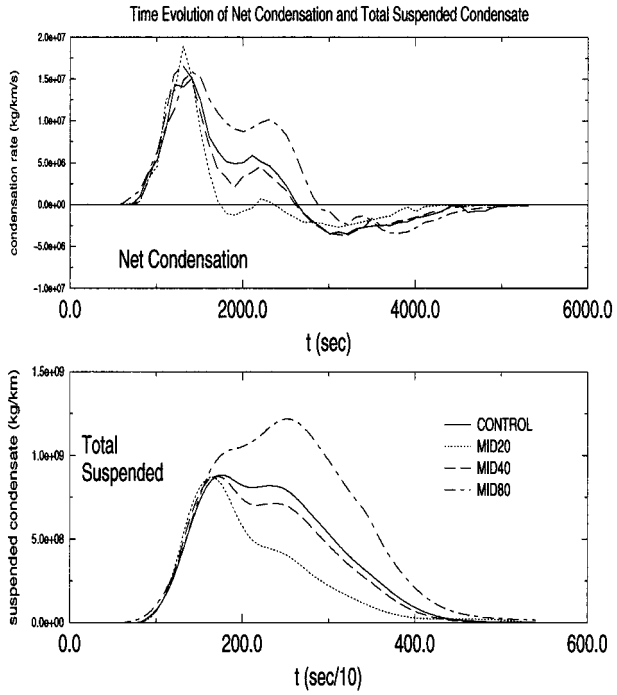

FIG. 13. Time series of net condensation (kg km^{-1}) and total suspended condensate (kg km^{-1}) for experiments CONTROL, MID20, MID40, and MID80.

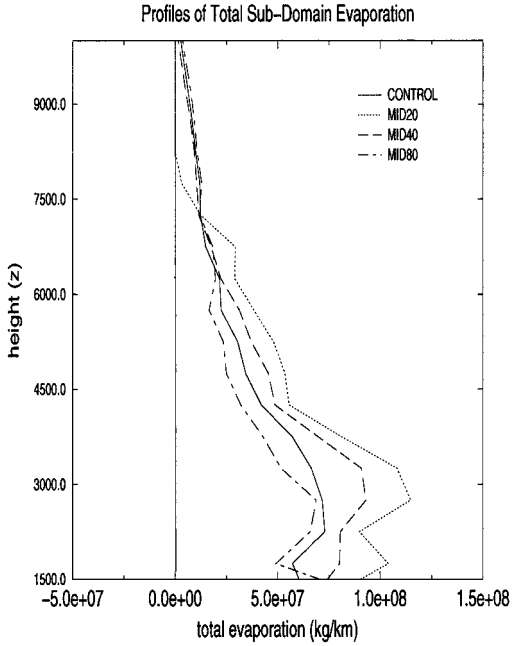

FIG. 14. Profiles of total evaporation (kg km^{-1}) from 1.5 (~850 mb) to 10.0 km in the subdomain for the 2D bulk moisture experiments. The 500-mb level is near 5.5 km.

density gradient between the boundary and inflow environment. The result was enhanced lifting at the outflow boundary. Lucas et al. (2000) also found stronger downdrafts in their drier runs. They similarly attributed this result to enhanced evaporational cooling of rainfall.

The forcing of stronger downdrafts by dry, midlevel environments is an active area of research. However, the important fact to observe is that the net condensation rates were similar between runs prior to 1500 s. The secondary maximum in net condensation near $t = 2200$ s for CONTROL, MID20, MID40, and MID80 was associated with secondary cell development. The results suggest that condensation associated with the secondary cell for MID80 is quite vigorous but significantly reduced for MID20. This explains why values of condensation in Table 6 are larger for MID80.

Arakawa and Schubert (1974), Simpson (1983), and Lucas et al. (2000) have all argued that entrainment reduces mass flux in clouds primarily by evaporating available liquid water in the cloud, cooling the parcel, and reducing buoyancy. This leads to lower rates of condensation. Examining the time series of total suspended condensate, results indicate that more hydrometeor species were suspended following $t = 2200$ s in MID80. Secondary cell development proceeded with less effect from evaporative processes. In the ''drier'' experiments, total suspended condensate exhibited a steady decay after an initial peak associated with the initial cell. Again, the suggestion is that drier midlevels promoted entrainment of dry air that evaporated water vapor in growing secondary convective cells and the initial mature cell. This limited the amount of suspended condensate (i.e., cloud water, ice, etc.) that could develop. Brown and Zhang (1997) inferred similar results in their investigation of cloud-top development in the warm pool region of the Pacific Ocean.

To investigate entrainment effects further, an analysis of cloud layer evaporation profiles was performed. Figure 14 displays profiles of total evaporation from the LCL to 10.0 km in the subdomain of this study. Compared to CONTROL, evaporative processes were larger below 500 mb in the drier experiments, such as MID20 and MID40, and smaller in MID80. Profiles of condensation and net condenastion (not shown) illustrated that drier experiments also produced net reductions in condensation between 850 and 500 mb. It is unclear whether evaporative or condensation processes were dominant but the net condensation profiles suggest that the evaporation term significantly altered the net condensation. These results also indicated that the *effects* of entrainment were greater when the 850–500-mb layer was drier, which served to inhibit secondary cell growth. This fact ultimately led to reduced precipitation efficiency and rainfall accumulations in the total system.

2) MOISTURE DISTRIBUTION EXPERIMENTS

Drier (moister) midlevels hinder (enhances) the development of rainfall by increasing (reducing) the effects of entrainment in the saturated updrafts that support cell development. Lin and Arakawa (1997a,b) and

TABLE 7. A description of the experiment, the precipitable water (mm) of the 850–500-mb layer (initial), and the CAPE (J kg^{-1}) of the prestorm environment for the moisture distribution experiments.

Expt	Mean 850–500-mb precipitable water (mm)	CAPE (J kg^{-1})
MOIST700500	22.4	1851
MOIST850700	22.0	1851
MOISTPAR	21.8	1851
DRY700500	15.1	1836
DRY850700	16.0	1836
DRYPAR	14.9	1836

Lucas et al. (2000) recently investigated what role the vertical distribution of moisture plays. Both investigators found that moistening of the lowest levels up to only 3.0 km was most critical. In Florida, observational studies (Frank and Smith 1968; Burpee 1979; Fuelberg and Biggar 1994) have consistently shown that midtropospheric moisture, specifically 700–500 mb (i.e., 3.0–5.5 km), exhibits strong correlations to rainfall activity in Florida. This study investigated the role of the moisture distribution using a set of experiments in which the vertical distribution of moisture was changed. Section 4 described the moisture distributions for each experiment.

Table 7 describes the experiments in terms of mean precipitable water and CAPE. CAPE values were fairly consistent for the dry and moist experiments, respectively. The initial precipitable water (PW, in mm) was calculated for the 850–500-mb layer for each of the distribution experiments. For all experiments in which water vapor was added (e.g., MOIST850700, MOIST700500, MOISTPAR), PW in the 850–500-mb layer was equal to 22.0, 22.4, and 21.8 mm, respectively. For all experiments in which water vapor was removed (e.g., DRY850700, DRY700500, DRYPAR), PW in the 850–500-mb layer was equal to 16.9, 15.1, and 14.9 mm, respectively. These results illustrate that though the 700–500-mb layer is thicker, it also contains less water vapor such that increases in relative humidity in this layer will generally be offset by the moister 850–700-mb layer, and vice versa. Since 850–500-mb water vapor was approximately constant over the range of experiments, it is instructive to see how the actual distribution in the layer affects rainfall evolution and secondary cell development.

Table 8 lists results for condensation, evaporation, total suspended condensate, rainfall amount, and precipitation efficiency. Examining the table, it is apparent that reducing moisture by similar amounts in the 850–700- or 700–500-mb layer produced roughly the same amount of rainfall and precipitation efficiency. However, the drier experiments generally produced 15% less rainfall and were less efficient rainfall producers than CONTROL, while the moist experiments generally produced on the order of 35% more rainfall and were slightly more efficient.

TABLE 8. A description of the model results from the moisture distribution experiments in terms of total condensation/deposition (C), total evaporation/sublimation (E), total surface rainfall (R), total suspended condensate (S), and precipitation effeciency (PE).

Expt	C (kg km^{-1}) $\times 10^8$	E (kg km^{-1}) $\times 10^8$	R (kg km^{-1}) $\times 10^8$	S (kg km^{-1}) $\times 10^8$	PE (%)
CONTROL	23.4	14.5	8.8	0.02	37
DRY850700	24.6	15.6	8.9	0.03	36
DRY700500	23.2	15.8	7.3	0.04	31
DRYPAR	24.5	16.8	7.7	0.01	32
MOIST850700	29.6	17.3	12.1	0.15	41
MOIST700500	26.6	14.8	11.6	0.07	44
MOISTPAR	23.8	13.6	10.1	0.04	43

In Fig. 15, as with the bulk moisture experiments, the initial rainfall evolution, depicted by the time series of precipitation efficiency, was quite similar in the distribution experiments. The experiments that were drier or moister in the 700–500-mb layer (e.g., DRYPAR, MOISTPAR, DRY700500, MOIST700500) exhibited the largest variability from CONTROL during secondary cell development after 2000 s.

Results in Table 8 indicate that similar variations in moisture in the upper or lower portion of the 850–500-mb layer altered rainfall totals. For example, increasing the moisture by similar amounts in the 850–700- (~1.5–3.0 km) or 700–500-mb layer (~3.0–5.5 km) produced roughly 36% more rainfall than CONTROL. Reducing the moisture in the same two layers had different effects. Decreasing the 700–500-mb layer moisture resulted in

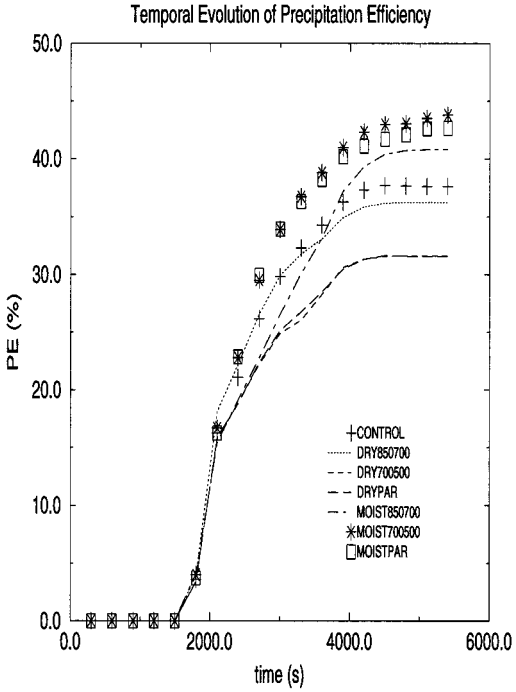

FIG. 15. Time series of precipitation efficiency (%) for 2D moisture distribution experiments.

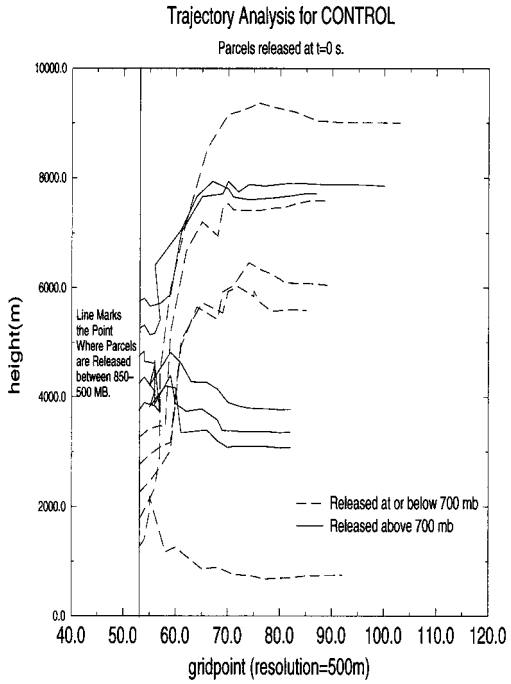

FIG. 16. Forward trajectory analysis of the CONTROL experiment. Parcels were released at $t = 0$ min and traced through $t = 90.0$ min.

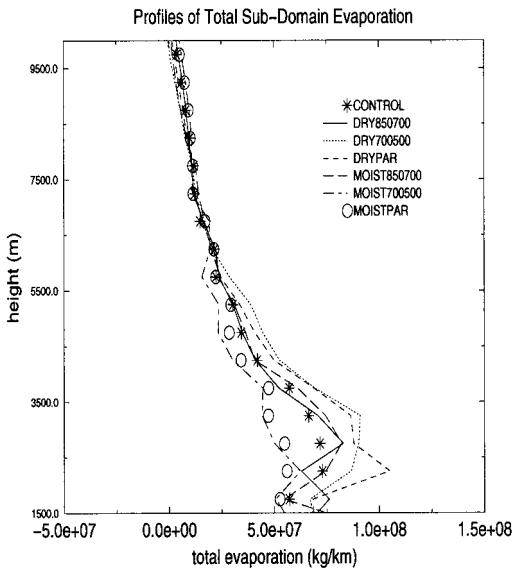

FIG. 17. Profiles of total evaporation (kg km^{-1}) from 1.5–10.0 km in the 2D moisture distribution experiments. Note: 850 mb ≅ 1.5 km, 700 mb ≅ 3.0 km, and 500 mb ≅ 5.5 km.

a 17% reduction in rainfall compared to CONTROL. There was virtually no change in rainfall when the 850–700-mb moisture was reduced. We suspect that the 850–700-mb layer is sufficiently moist that the sensitivity variations used were not sufficient to perturb rainfall amounts. These results suggest *that moistening or drying the atmosphere from 3.0 to 5.5 km can significantly impact rainfall.* This is different from Lin and Arakawa (1997a) and Lucas et al. (2000) who found that moisture up to roughly 3.0 km was critical to explain variability in convection through moisture distribution changes. Both of these studies examined long-lived, oceanic squall systems with low cloud bases and large wind shear environments. In such environments, upshear-tilted systems may likely be affected more by lower-level moisture. In the quasi-stationary convergence zone systems of this study, the convection was relatively short lived (~0.5–2.0 h) and associated with weak wind shear and higher cloud bases. Additionally, the storms were virtually erect and possibly even downshear tilted. A westerly wind aloft also ''blew through'' the storm, which is essentially stationary relative to the initial convergence point. Ferrier et al. (1996) found that erect storms in moist midlevel environments were more efficient at producing rainfall. Our findings along with Ferrier et al. (1996) indicate *that the typically erect storms of the Florida convergence zone environment may be significantly hindered by entrainment effects from dry midtroposheric air.*

Using the forward trajectory analysis of Tao et al. (1995), parcels were released at various levels in the 850–500-mb layer east of the eventual cloud region at $t = 0$ s and followed for 1.5 h. It is shown that air parcels penetrated the cloud region (1.5–10.0 km) from all levels below 500 mb. Forward trajectories were calculated for the CONTROL experiment (Fig. 16) to illustrate that air parcels may enter the cloudy region of a growing cell from levels ranging from 850 to 500 mb. Figure 16 illustrates that some parcels in the 850–700-mb layer are entrained into the updraft region and detrained at 7.0–9.0 km. Other parcels were transported downward. Parcels between 3.6 and 4.7 km were entrained into the updraft region but exit the cloud region near 3.0–3.3 km. This suggests that air above 700 mb can be transported downstream and to lower levels (i.e., above the outflow boundary) where secondary cell development is favored. Parcels in the upper layer of the 700–500-mb layer can also be entrained into the system's updraft and detrained near 9.0 km. The 700–500-mb layer can exert as much control over updraft and secondary cell evolution as the 850–700-mb layer.

Profiles of total evaporation in Fig. 17 illustrate that most of the variability in evaporation occurred below 6.0 km. Above this level, evaporation profiles were quite similar. The experiments that produced the largest increases in evaporation relative to CONTROL were DRY700500 and DRYPAR. The net increases were as large as 30%–50% and peaked between 2200 and 3300 m. This indicates that dry environmental air above 3.0 km was likely entraining into regions below 3.0 km to promote evaporation of developing secondary cells. Similarly, the largest reductions in evaporation were observed in MOIST700500 and MOISTPAR. This indicates that the effects of air entraining from the 700–500-mb level were not as detrimental for secondary cell

growth when the upper layer was moist. Observing the profiles of MOIST850700 and DRY850700, they behaved quite similarly to CONTROL. This would indicate that evaporative effects are more influential for a dry 700–500-mb layer. This finding is consistent with Frank and Smith (1968), Burpee (1989), Watson et al. (1991), and Fuelberg and Biggar (1994).

Moisture variability from 850 to 500 mb (~1.5–5.5 km) in summertime Florida affects rainfall production in convergence zone systems. Since low-level moisture is virtually ubiquitous in Florida in the summer months, these results explain why midtropospheric moisture exhibits a strong statistical correlation to rainfall. *The midtropospheric moisture is likely to exhibit a wider range in variability that is correlative with rainfall variability.*

c. Conceptualization of rainfall evolution in convergence zone systems in Florida

Since the atmosphere is three-dimensional, not two-dimensional, a subset of 3D runs were done to verify the 2D modeling results *though they were not meant to be exhaustive.* The 3D results will not be discussed in this manuscript but will be addressed in future papers. Generally, the 3D results were in complete agreement with the 2D results. *Examining the respective 3D systems toward the latter stages of their life cycle, it can be inferred that vertical moisture flux played a decreasing role as the system matures, while midtropospheric moisture played an increasing role.*

The goal now is to tie the results together into a coherent picture of the evolution of convective rainfall forced by a typical Florida convergence zone interaction (i.e., an SBF–OB collision). Recently, Fovell and Tan (1998) presented a theoretical description of cell evolution in a multicell system. They suggested that the buoyancy-induced circulations associated with developing cells may entrain environmental air. Dry air in the 850–500-mb layer could reduce the buoyancy-induced circulation as air is entrained from the sides and the top of the newly generated cell. Evidence from this study and similar work by Ferrier and Houze (1989) confirmed that secondary cell responds strongly to the environmental moisture in the 850–500-mb layer.

Figure 18 is a schematic that illustrates the general findings of this study. The time history of cell evolution in a typical multicell system is presented along the ordinate. It is essentially a depiction of time evolution. The abcissa rates the relative influence of vertical moisture flux forcing and midtropospheric moisture. *In Fig. 18, it is suggested that vertical moisture flux forcing associated with the collision of the OB and SBF exerts a stronger influence on the initial cell, associated primarily with early rainfall totals. However, this influence decreases with time as secondary cells evolve. Environmental moisture in the midtroposphere takes on a stronger influence as secondary cells evolve. The moisture regulates the decay of the initial cell once the initial burst of rainfall linked to VMF forcing subsides. More importantly, the moisture regulates how effectively secondary cells evolve.* Future work should investigate this theory under different synoptic patterns and wind shear regimes.

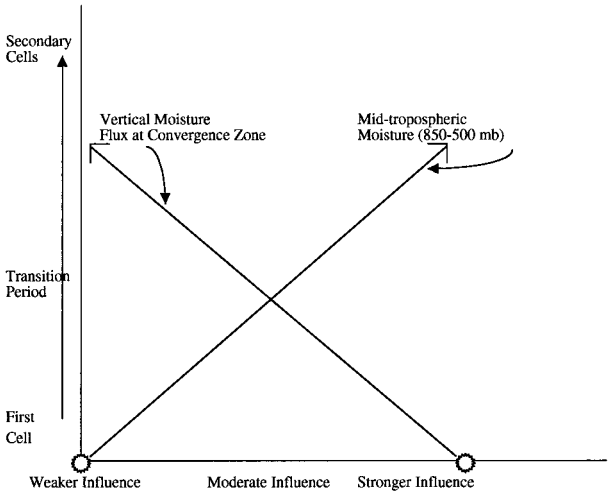

FIG. 18. Schematic of the influence of vertical moisture flux and midtropospheric moisture on rainfall evolution. The ordinate represents time evolution of cell development. The abscissa represents relative influence of vertical moisture flux and moisture. The open starburst represents the starting point along each influence line.

6. Summary and conclusions

The purpose of this study to identify and quantify how rainfall development (i.e., initial rainfall, total amount, precipitation efficiency) at a typical Florida convergence zone is influenced by the observationally significant low-level convergence and midtropospheric moisture fields. This research was different from many previous studies in that the focus was on rainfall morphology at convergence zones, not convective initiation.

a. Conclusions

It was found that initial rainfall morphology is related not only to the amount of low-level convergence but to the depth of the convergence. This extends earlier studies like Ulanski and Garstang (1978) and Tripoli and Cotton (1980) that linked Florida rainfall to magnitude and areal extent of *surface* convergence only. The magnitude and depth of convergence was quantified as a vertical moisture flux parameter. There were direct, linear relationships between the area- and time-averaged vertical moisture flux at the outflow boundary–seabreeze front convergence zone and the initial condensation rates of the first convective cell. This relationship established a similar relationship with initial rainfall rates and accumulations produced by the first cell. Increasing (decreasing) area- and time-averaged vertical moisture flux over an observable range of convergence

zone conditions produced variability in initial rainfall on the order of ±25%. Weaker correlations existed between area- and time-averaged surface convergence and initial rainfall.

Secondary cell development and rainfall production was found to be directly related to how the 850–500-mb moisture content affects entrainment effects (i.e., rates of evaporation and condensation). For the observable range (±20%) of variance in relative humidity in the midtroposphere (850–500 mb), precipitation efficiency (calculated from total condensation and rainfall not cloud base or surface inflow) varied from 23% to 47% while total rainfall accumulation varied by almost a factor of 2. The bulk changes in moisture produced relatively large variations in precipitation efficiency and total rainfall amount, but initial rainfall evolved in roughly the same manner. Results quantify, using models, what numerous investigators have observed in Florida systems.

Rainfall from the initial cell responded to a given vertical moisture flux, but, the total rainfall was regulated by the ambient 850–500-mb moisture. The dry midtropospheric experiments produced significantly weaker secondary convective cells, while the moist experiments produced vigorous secondary cell development. This fact was indicated by evidence of relatively high net condensation rates and suspended condensate after the initial cell in the ''moist'' experiments. Likewise, ''drier'' experiments produced larger reductions in net condensation and suspended condensate following the initial cell, which indicated that secondary convective activity was being reduced by evaporation processes. The evidence indicates that drier (moister) midlevels hinders (enhances) the development of rainfall by increasing (reducing) the effects of entrainment in the saturated updrafts.

The study also revealed that drying or moistening the 850–700- or 700–500-mb layer by comparable amounts produced similar variations in rainfall production and efficiency. Moisture variability in the 3.0–5.5-km layer can affect rainfall as much as moisture variability at lower levels. This is different from Lin and Arakawa (1997a) and Lucas et al. (2000) who found that moisture up to roughly 3.0 km was critical for explaining variability in convection through moisture distribution changes. Both of those studies examined long-lived, oceanic convection with low cloud bases, larger wind shear environments, and moving cloud systems. In such environments, upshear-tilted systems may likely be affected more by lower-level moisture. In the convergence zone systems of this study, there was weak wind shear and higher cloud bases. Additionally, the storms were virtually erect and possibly even downshear tilted. All of these factors are theorized to play a role in allowing the midtroposphere to exert significant influence on entrainment-related effects like cloud evaporation and condensation rates. Since low-level moisture is virtually ubiquitous in Florida in the summer months, this study explains why midtropospheric (700–500 mb) moisture exhibits a strong statistical correlation to rainfall in previous observational work. Midtropospheric moisture is likely to exhibit a wider range of variability, whereas lower-level moisture is virtually always present.

b. Implications

This study unified two schools of observation (i.e., low-level convergence and midtropospheric moisture) concerning the production of rainfall in small, Florida convective systems. Additionally, the research provided an assessment of the precipitation efficiency and rainfall potential of these systems. This work also extended the body of numerical modeling studies of Florida convection at the convective–mesogamma scale. This study also highlighted the need for improved measurement of convergence parameters, and midtropospheric moisture distribution at these scales. It was revealed that the environment needs to be better represented in convective parameterizations of larger-scale models to account for entrainment effects. Furthermore, the results suggest that the nature of the role of entrainment effects and ambient moisture in convection may differ for storms depending on several factors. Such factors include whether they are short-lived or long-lived systems, oceanic- or land-based systems, erect or tilted systems, or systems embedded in weak or strong shear environments. All of these areas are appropriate for future investigations.

Acknowledgments. This research was sponsored by the National Aeronautics and Space Administration Goddard Space Flight Center Research and Study Fellowship. The authors are grateful to B. Adler, F. Einaudi, V. Salomonson, E. Smith, H. Fuelberg, T. N. Krishnamurti, R. Krishnamurti, and D. Menchan for their support. Thanks are also due to B. Lynn for the providing the satellite data and the ARPS Group at CAPS for providing the model and insight concerning its use. We are also thankful to our colleagues who provided helpful comments and suggestions during the review of this manuscript.

REFERENCES

Arakawa, A., and W. H. Schubert, 1974: Interaction of a cumulus cloud ensemble with the large scale environment. Part I. *J. Atmos. Sci.,* **31,** 674–701.

Arritt, R. W., 1993: Effects of the large-scale flow on characteristic features of the sea breeze. *J. Appl. Meteor.,* **32,** 116–125.

Blanchard, D. O., and R. E. Lopez, 1985: Spatial patterns of convection in south Florida. *Mon. Wea. Rev.,* **113,** 1282–1299.

Blyth, A. M., 1993: Entrainment in cumulus clouds. *J. Appl. Meteor.,* **32,** 626–641.

Braham, R. R., 1952: The water and energy budgets of the thunderstorm and their relation to thunderstorm development. *J. Meteor.,* **9,** 227–242.

Brown, R. G., and C. Zhang, 1997: Variability of midtropospheric moisture and its effects on cloud-top height distribution during TOGA COARE. *J. Atmos. Sci.,* **54,** 2760–2774.

Browning, K. A., and Coauthors, 1976: Structure of an evolving hailstorm. Part V: Synthesis and implications for hail growth and hail suprression. *Mon. Wea. Rev.,* **104,** 603–610.

Burpee, R. W., 1979: Peninsula-scale convergence in the south Florida sea breeze. *Mon. Wea. Rev.,* **107,** 852–860.

——, 1989: A summer day without significant rainfall in south Florida. *Mon. Wea. Rev.,* **117,** 680–687.

Byers, H. R., and H. R. Rodebush, 1948: Causes of thunderstorms of the Florida peninsula. *J. Meteor.*, **5,** 275–280.

——, and R. R. Braham Jr., 1949: *The Thunderstorm.* U.S. Govt. Printing Office, 287 pp.

Charba, J., 1974: Application of gravity current model to analysis of a squall-line gust front. *Mon. Wea. Rev.,* **102,** 140–156.

Chen, C., 1995: Numerical simulations of gravity currents in uniform shear flows. *Mon. Wea. Rev.,* **123,** 3240–3253.

Cooper, H. J., M. Garstang, and J. Simpson, 1982: The diurnal interaction between convection and peninsular-scale forcing over South Florida. *Mon. Wea. Rev.,* **110,** 486–503.

Crook, N. A., 1996: Sensitivity of moist convection forced by boundary layer processes to low-level thermodynamic fields. *Mon. Wea. Rev.,* **124,** 1767–1785.

Day, S., 1953: Horizontal convergence and the occurrence of summer shower precipitation at Miami, Florida. *Mon. Wea. Rev.,* **81,** 155–161.

Droegemeier, K. K., and R. B. Wilhelmson, 1985: Three-dimensional numerical modeling of convection produced by interacting thunderstorm outflows. Part I: Control simulation and low-level moisture variations. *J. Atmos. Sci.,* **42,** 2381–2403.

Fankhauser, J. C., N. A. Crook, J. Tuttle, L. J. Miller, and C. G. Wade, 1995: Initiation of deep convection along boundary layer convergence lines in a semitropical environment. *Mon. Wea. Rev.,* **123,** 291–313.

Ferrier, B. S., and R. A. Houze Jr., 1989: One-dimensional time-dependent modeling of GATE cumulonimbus convection. *J. Atmos. Sci.,* **46,** 330–352.

——, J. Simpson, and W. K. Tao, 1996: Factors responsible for precipitation efficiencies in midlatitude and tropical squall simulations. *Mon. Wea. Rev.,* **124,** 2100–2125.

Fovell, R. G., and P. H. Tan, 1998: The temporal behavior of numerically simulated multicell-type storms. Part II: The convective cell life cycle and cell regeneration. *Mon. Wea. Rev.,* **126,** 551–577.

Frank, N. L., and D. L. Smith, 1968: On the correlation of radar echoes over Florida with various meteorological parameters. *J. Appl. Meteor.,* **7,** 712–714.

——, P. L. Moore, and G. E. Fisher, 1967: Summer shower distribution over the Florida peninsula as deduced from digitized radar data. *J. Appl. Meteor.,* **6,** 309–316.

Fuelberg, H. E., and D. Biggar, 1994: The preconvective environment of summer thunderstorms over the Florida panhandle. *Wea. Forecasting,* **9,** 316–326.

Gentry, R. C., and P. L. Moore, 1954: Relation of local and general wind interaction near the sea coast to time and location of airmass showers. *J. Meteor.,* **11,** 507–511.

Halverson, J., M. Garstang, J. Scale, and W.-K. Tao, 1996: Water and energy budgets of a Florida mesoscale convective system: A combined observational and modeling study. *Mon. Wea. Rev.,* **124,** 1161–1180.

Heymsfield, G. M., I. J. Caylor, J. M. Shepherd, W. S. Olson, S. W. Bidwell, W. C. Boncyk, and S. Ameen, 1996: Structure of Florida thunderstorms using high-altitude aircraft radiometer and radar observations. *J. Appl. Meteor.,* **35,** 1736–1762.

Holle, R. L., and A. I. Watson, 1983: Duration of convective events related to visible cloud, convergence, radar and raingage parameters in south Florida. *Mon. Wea. Rev.,* **111,** 1046–1051.

Hondl, K. D., and M. D. Eilts, 1994: Doppler radar signatures of developing thunderstorms and their potential to indicate the onset of cloud-to-ground lightning. *Mon. Wea. Rev.,* **122,** 1818–1836.

Kingsmill, D., 1995: Convection initiation associated with a sea-breeze front, a gust front, and their collision. *Mon. Wea. Rev.,* **123,** 2913–2933.

Lee, B. D., R. D. Farley, and M. R. Hjelmelt, 1991: A numerical case study of convection initiation along colliding convergence boundaries in northeast Colorado. *J. Atmos. Sci.,* **48,** 2350–2366.

Lin, C., and A. Arakawa, 1997a: The macroscopic entrainment processes of simulated cumulus ensemble. Part I: Entrainment sources. *J. Atmos. Sci.,* **54,** 1027–1043.

——, and ——, 1997b: The macroscopic entrainment processes of simulated cumulus ensemble. Part II: Testing the entraining plume model. *J. Atmos. Sci.,* **54,** 1044–1053.

Lopez, R. E., P. T. Gannon, D. O. Blanchard, and C. C. Balch, 1984: Synoptic and regional circulation parameters associated with the degree of convective shower activity in south Florida. *Mon. Wea. Rev.,* **112,** 686–703.

Lucas, C., E. J. Zipser, and B. S. Ferrier, 2000: Sensitivity of tropical west Pacific oceanic squall lines to tropospheric winds and moisture profiles. *J. Atmos. Sci.,* **57,** 2351–2373.

McIlveen, J. F. R., 1986: *Basic Meteorology—A Physical Outline.* Van Nostrand Reinhold, 457 pp.

Moore, J. T., 1982: The forcing and evolution of the three dimensional moisture convergence during the 10–11 April 1979 severe weather outbreak. Preprints, *12th Conf. on Severe Local Storms,* San Antonio, TX, Amer. Meteor. Soc., 209–212.

Mueller, C. K., J. W. Wilson, and N. A. Crook, 1993: The utility of sounding and mesonet data to nowcast thunderstorm initiation. *Wea. Forecasting,* **8,** 132–146.

Nicholls, M. E., R. A. Pielke, and W. R. Cotton, 1991: A two-dimensional numerical investigation of the interaction between sea breezes and deep convection over the Florida peninsula. *Mon. Wea. Rev.,* **119,** 298–323.

Pielke, R., 1974: A three-dimensional model of the seabreeze over south Florida. *Mon. Wea. Rev.,* **102,** 115–139.

Rao, P. A., H. E. Fuelberg, and K. K. Droegemeier, 1999: High resolution modeling of the Cape Canaveral area land/water circulations and associated features. *Mon. Wea. Rev.,* **127,** 1808–1821.

Simpson, J., 1983: Cumulus clouds: Early aircraft observations and entrainment hypotheses. *Mesoscale Meteorology—Theories, Observations and Models,* D. K. Lilly and T. Gal-Chen, Eds., D. Riedel, 355–373.

Simpson, J. E., 1987: *Gravity Currents: In the Environment and the Laboratory.* John Wiley and Sons, 244 pp.

——, N. E. Westcott, R. J. Clerman, and R. A. Pielke, 1980: On cumulus mergers. *Arch. Meteor. Geophys. Bioklimatol.,* **A29,** 1–40.

——, C. Kummerow, W.-K. Tao, and R. F. Adler, 1996: On the Tropical Rainfall Measuring Mission (TRMM). *Meteor. Atmos. Phys.,* **60,** 19–36.

Stommel, H., 1947: Entrainment of air into a cumulus cloud. *J. Meteor.,* **4,** 91–94.

Sun, J., and N. A. Crook, 1998: Dynamical and microphysical retrieval from Doppler radar observations using a cloud model and its adjoint. Part II: Retrieval experiments of an observed Florida convective storm. *J. Atmos. Sci.,* **55,** 835–852.

Tao, W. K., J. R. Scala, B. Ferrier, and J. Simpson, 1995: The effect of melting processes on the development of a tropical and a midlatitude squall line. *J. Atmos. Sci.,* **52,** 1934–1948.

Tripoli, G. J., and W. R. Cotton, 1980: A numerical investigation of several factors contributing to the observed variable intensity of deep convection over south Florida. *J. Appl. Meteor.,* **19,** 1037–1063.

Ulanski, S. L., and M. Garstang, 1978: The role of surface divergence and vorticity in the life cycle of convective rainfall. Part I: Observation and analysis. *J. Atmos. Sci.,* **35,** 1047–1062.

Wakimoto, R., and D. E. Kingsmill, 1995: Structure of an atmospheric undular bore generated from colliding boundaries during CaPE. *Mon. Wea. Rev.,* **123,** 1374–1393.

Watson, A. I., and D. O. Blanchard, 1984: The relationship between

total area divergence and convective precipitation in south Florida. *Mon. Wea. Rev.*, **112,** 673–685.

——, R. L. Holle, R. E. Lopez, R. Ortiz, and J. R. Nicholson, 1991: Surface wind convergence as a short term predictor of cloud-to-ground lightning at Kennedy Space Center. *Wea. Forecasting*, **6,** 49–64.

Weisman, M. L., and J. B. Klemp, 1982: The dependence of numerically simulated convective storms on vertical wind shear and buoyancy. *Mon. Wea. Rev.*, **110,** 504–520.

Williams, S., K. Caeser, and K. Southwick, 1992: Convection and Precipitation Experiment operations summary and data inventory. Office of Field Project Support, Boulder, CO, 425 pp.

Wilson, J. W., and D. L. Megenhardt, 1997: Thunderstorm initiation, organization, and lifetime associated with Florida boundary convergence lines. *Mon. Wea. Rev.*, **125,** 1507–1525.

Xin, L., and G. W. Reuter, 1996: Numerical simulation of the effects of mesoscale convergence on convective rain showers. *Mon. Wea. Rev.*, **124,** 2828–2842.

Xue, M., K. K. Droegemeier, V. Wong, A. Shapiro, and K. Brewster, 1995: ARPS version 4.0 user's guide. Center for Analysis and Prediction of Storms, 380 pp. [Available from Center for Analysis and Prediction of Storms, University of Oklahoma, Norman, OK 73019-1011.]

Yuter, S. E., and R. A. Houze Jr., 1995: Three-dimensional kinematic and microphysical evolution of Florida cumulonimbus. Part I: Spatial distribution of updrafts, downdrafts, and precipitation. *Mon. Wea. Rev.*, **123,** 1921–1940.